ACS APPLIED MATERIALS & INTERFACES

Research Article

www.acsami.org

Novel Carrier Doping Mechanism for Transparent Conductor: Electron Donation from Embedded Ag Nanoparticles to the Oxide Matrix

Po-Shun Huang,[†] Fen Qin,[†] Ziye Xiong,[†] Hyun-Woo Shim,[†] Tongchuan Gao,[‡] Paul Leu,[‡] and Jung-Kun Lee*[,†]

[†]Department of Mechanical Engineering and Materials Science, University of Pittsburgh, Pittsburgh, Pennsylvania 15261, United States

[‡]Department of Industrial Engineering, University of Pittsburgh, Pittsburgh, Pennsylvania 15261, United States

Supporting Information

ABSTRACT: A trade-off between the carrier concentration and carrier mobility is an inherent problem of traditional transparent conducting oxide (TCO) films. In this study, we demonstrate that the electron concentration of TCO films can be increased without deteriorating the carrier mobility by embedding Ag nanoparticles (NPs) into Al-doped ZnO (AZO) films. An increment of Ag NP content up to 0.7 vol % in the AZO causes the electron concentration rising to 4×10^{20} cm^{-3}. A dependence of the conductivity on temperature suggests that the energy barrier for the electron donation from Ag NPs at room temperature is similar to the Schottky barrier height at the Ag−AZO interface. In spite of an increase in the electron concentration, embedded Ag NPs do not compromise the carrier mobility at room temperature. This is evidence showing that this electron donation mechanism by Ag NPs is different from impurity doping, which produces both electrons and ionized scattering centers. Instead, an increase in the Fermi energy level of the AZO matrix partially neutralizes Al impurities, and the carrier mobility of Ag NP embedded AZO film is slightly increased. The optical transmittance of mixture films with resistivity less than 1×10^{-3} Ω·cm still maintains above 85% in visible wavelengths. This opens a new paradigm to the design of alternative TCO composite materials which circumvent an inherent problem of the impurity doping.

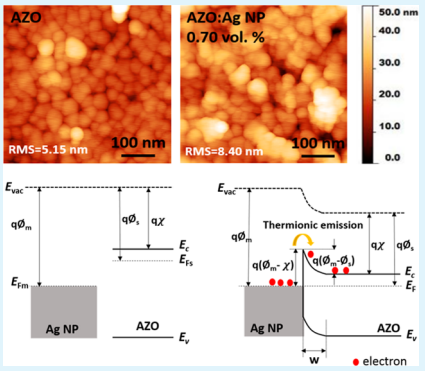

KEYWORDS: *silver nanoparticle, aluminum-doped ZnO, metal−metal oxide interface, electron transfer, transparent conducting oxide film*

INTRODUCTION

Transparent conducting oxides (TCOs) are wide band gap (>3.0 eV) materials doped with a certain amount of shallow donors or acceptors. Therefore, they exhibit high electrical conductivity and excellent optical transparency, which are required for transparent electrode materials in the field of optoelectronics. Indium tin oxide (ITO) film is a well-known TCO, and its sheet resistivity and transmittance can be 2×10^{-4} Ω·cm and above 80% for the visible light. Although ITO has such attractive electrical and optical properties, there are several issues such as the scarcity of elemental indium. Also, the brittleness of ITO limits its application to polymer substrates for flexible electronics. These problems have rekindled research interests on new TCO materials. A common and effective way to improve the electric conductivity of degenerated semiconductors such as TCOs is to increase carrier concentration by adding more localized shallow donor states.[1−9] However, the heavy doping of impurities results in a trade-off between the carrier concentration and the electron mobility because charged impurities work as scattering centers of carriers. Therefore, the carrier mobility is decreased, and the electric conductivity in heavily doped TCOs is saturated.[10] Moreover, excessively doped impurities can also form color centers that often reduce the light transmittance through the TCO film.

To circumvent this correlation between the carrier concentration, mobility, and the optical transmittance, carrier doping without adding impurities has been pursued. Cohen and Barnett proposed a simulated structure originated from the modulation doping, which consists of two alternating semiconducting layers:[11,12] the heavily doped layer provides conducting electrons to the lightly doped layer, where electrons can travel without the impurity scattering. Although this type of electron donation predicts the high carrier mobility in the semiconductor with the high electron concentration, experimental validation has not been fully performed yet. In the past few years, electrical and optical properties of electron-rich metal films or nanowire/TCO composite films have been studied.[13−19] Their results indicate that electrons travel only

Received: April 3, 2017
Accepted: May 22, 2017
Published: May 22, 2017

DOI: 10.1021/acsami.7b03871
ACS Appl. Mater. Interfaces 2017, 9, 19973−19979

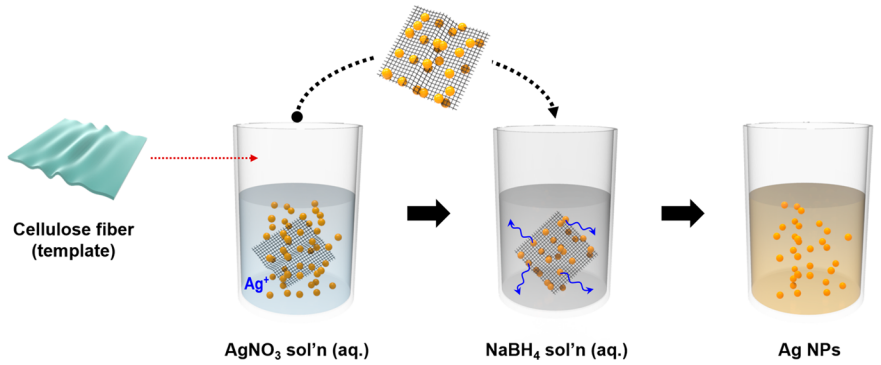

Figure 1. Illustration of the Ag NP synthesis with assistance of cellulose fibers.

through the metal film or the interconnected network of the nanowires (NWs), which results in the poor carrier mobility of ~10 cm^2 $V^{-1}·s^{-1}$ due to the scattering at the interface of the metal constituent and the TCO layer. Moreover, the optical transmittance of such composite films decreases significantly down to 60% or lower, as the thickness of the metal layer or the amount of the nanowires in the composite film increases for high electric conductivity.[20] In terms of electron transport behavior, the metal NW/TCO composite films are comparable to the TCO/metal/TCO sandwiched films because their metal constituents form a percolation path that allows electrons to go through the metal network. A minimum amount of NWs that can create the percolation path is 0.5−1.0 vol % in the NW-based composite system, which depends on the aspect ratio of the metal nanowires.[20,21] On the other hand, we recently reported the electric properties of ZnO/Au/ZnO multilayer film grown by e-beam and sol−gel methods. When the Au layer was thermally annealed to form isolated Au nanoparticles (Au NPs) in ZnO matrix, the thermionic emission of electrons from Au NPs to ZnO occurred, and the electron concentration increased.[22] This mechanism is different from the metal nanowire-based TCOs, where the NWs work as a highway for electron transport.

In the present study, we demonstrate that metal nanoparticles (NPs) embedded in Al-doped ZnO (AZO) film can increase the carrier concentration of AZO matrix. Due to a difficulty in controlling the formation of inherent defects (oxygen vacancy and zinc interstitials) in pure ZnO, we chose AZO with a controlled impurity concentration (Al in Zn site) as a matrix material. A source of n-type conductivity and major types of defects are well-known in Al-doped ZnO. In this way, any increments of electron concentrations will be directly related to the Ag nanoparticles. Ag NPs-AZO film is fabricated via wet solution method, which offers a better controllability over the size and the distribution of Ag NPs in the AZO matrix in comparison with that of physical or chemical vapor deposition techniques. Because a small amount of well-distributed Ag NPs is not physically connected, the effect of the Ag NPs on the conductivity of the TCO matrix is not due to the percolation of NPs. The increased electric conductivity of Ag NPs embedded AZO is explained using the electron donation at Ag−AZO interface where the Schottky barrier serves as an energetic barrier height.

RESULTS AND DISCUSSION

A synthesis of Ag NPs with assistance of cellulose fibers is illustrated in Figure 1. The size and morphology of Ag NPs grown on the cellulose fibers were first examined using several characterization tools. Figures 2a and b show the transmission electron microscopy (TEM) image of Ag NPs and the particle

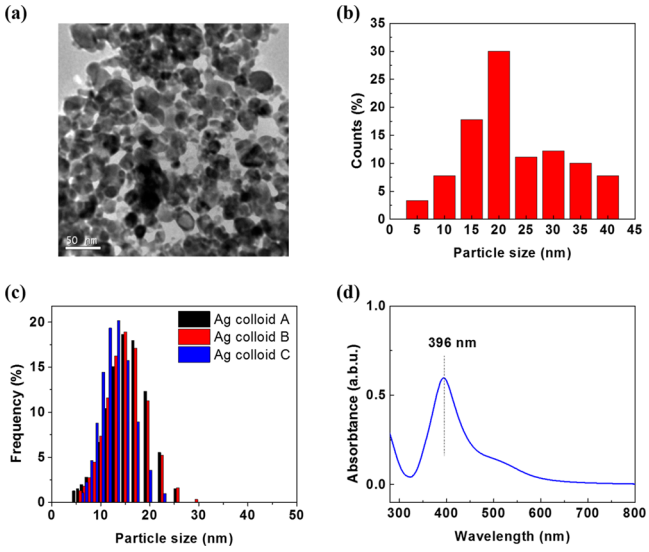

Figure 2. (a) TEM image of as-synthesized Ag NPs. (b) Size analysis of Ag NPs based on the TEM image. (c) Size distribution of Ag colloids obtained from DLS measurement (initial silver ion concentration in the solution vary: colloid A, 0.01 M; colloid B, 0.1 M; colloid C, 0.5 M) and (d) UV−vis spectrum of Ag NPs in 2-methoxyethanol.

size distribution obtained from the TEM image. The particle size was 21 ± 8.0 nm. In addition, the size distribution of Ag NPs in the AZO solutions with different amounts of Ag NPs was measured by dynamic light scattering (DLS). As shown in Figure 2c, the size of Ag NPs ranges from 5 to 30 nm with an average of 15 nm regardless of initial Ag concentrations (0.01 ~ 0.05 M) in colloidal solutions. Results of TEM and DLS analyses indicates that use of cellulose fibers during the reduction process results in Ag NPs with the uniform size of 15−20 nm. A moderate release of Ag ions from the cellulose fibers into the reducing media results in slow and uniform reduction of Ag NPs. The size of Ag NPs was also confirmed using UV−vis spectroscopy. All Ag NPs solutions synthesized from precursors with different Ag ion concentrations exhibit a similar absorption peak sharp surface plasmonic absorption at λ = 395 nm. Figure 2d shows a characteristic peak of Ag NPs with the size of about 20 nm.

The compositions of Ag NP added AZO films were measured by electron probe micro-analyzer (EPMA) and X-

DOI: 10.1021/acsami.7b03871
ACS Appl. Mater. Interfaces 2017, 9, 19973−19979

ray photoelectron spectroscopy (XPS) measurements. The ratio of Ag/Zn ratios obtained from EPMA and XPS were all converted into the volume ratios (vol %). Ag contents of the mixture films from EPMA and XPS were fairly consistent (Table 1). Given that XPS is very sensitive to the film surface

Table 1. Electrical Resistivity of Mixture Films with Regard to the Ag Content

sample	Ag content by EPMA (vol %)	Ag content by XPS (vol %)	resistivity (Ω·cm)
AZO			1.85×10^{-2}
A	0.07	0.14	8.62×10^{-3}
B	0.35	0.37	2.72×10^{-3}
C	0.70	0.68	9.60×10^{-4}
pure ZnO			8.2×10^{-1}
D	0.70	0.72	1.56×10^{-3}

(~10 nm depth) and EPMA collects signals from the entire film with 200 nm thickness, the consistency of the two measurements suggests that the Ag NPs are well-dispersed in the AZO matrix. The diffusion of Ag to the film surface during the thermal annealing was not observed in this study. In addition to the composition, the oxidation state of Ag NPs embedded in the AZO matrix was examined by XPS. The XPS analysis was conducted after Ar^+ ion sputtering for 10 s in order to remove undesired native oxide or another contamination layer on the surface. XPS spectra of the mixture films are shown in Figure 3. Photoemission peaks of the mixture films are

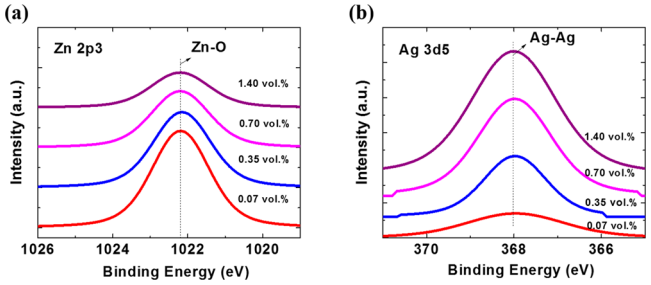

Figure 3. Chemical analysis for (a) Zn $2p_{3/2}$ and (b) Ag $3d_{5/2}$ of the AZO:Ag NP mixture films.

centered at 368.04 eV in all mixture films with different Ag NP content. Peak positions are corrected using C 1s peak as an internal reference. This peak corresponds to the binding energy (BE) of electrons at Ag $3d_{5/2}$ level and shift of BE, which is a proof of Ag−O bonding was not observed. The XPS analysis indicates that Ag NPs are in the metallic state even after the heat treatment. This is because Ag is inert, and AZO matrix shields Ag NPs from the ambience. Therefore, an oxidation reaction of Ag NPs is retarded. Surface morphologies of the thermally annealed mixture films are examined by AFM. As shown in Figure 4, all mixture films have a similar microstructure with the average grain size of ~50 nm. The surface roughness of the mixture films characterized by an average root-mean-square (RMS) value did not show a significant difference as a function of Ag NP content. This suggests the addition of a small amount of Ag NPs into AZO film does not influence the microstructure of the mixture films, and light scattering at the surface and grain boundary is similar in pure and Ag NP added AZO films. Grazing-angle X-ray diffractions (GAXRD)

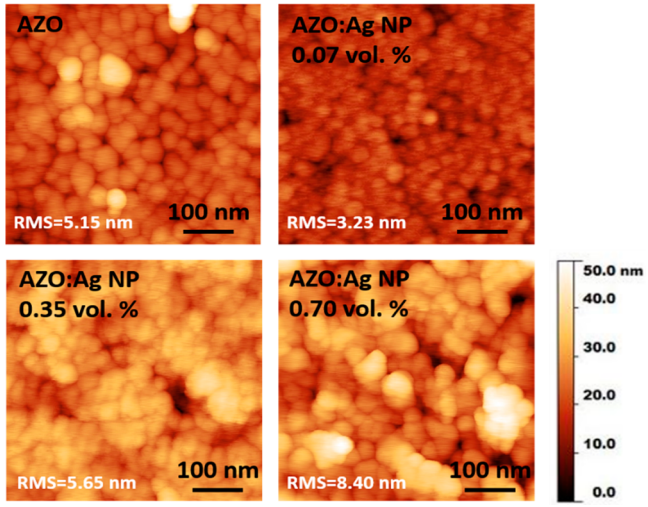

Figure 4. AFM image reveals the morphologies of the mixture films with varied Ag content.

measurements were performed at the incident angle of 0.1° for pure and Ag NP added AZO films. GAXRD patterns are represented in Figure S2. All mixture films exhibit the same peaks that are indexed as wurtzite phase of ZnO. As Ag NP content increases, (111) peak of cubic Ag appears at $2\theta = 44.6°$. These GAXRD results suggest that AZO matrix has the polycrystalline structure of wurtzite ZnO and that Ag forms nanoparticles instead being incorporated in the AZO matrix.

Table 1 shows the effect of Ag NP addition on the electric properties of AZO film at room temperature as a function of Ag NP content. Measurements were performed in a dark condition to exclude the possibility of electron emission from surface plasmonic resonance. Though the resistivity of PLD grown AZO film can be as low as 3×10^{-4} Ω·cm, the resistivity of sol−gel grown AZD films is higher than that of PLD grown ALD film. The addition of Ag NPs decreases the resistivity of the films. The resistivity of 0.7 vol % Ag NP:AZO film is 20 times smaller than that of pure AZO film. A decrease in the resistivity of Ag NP:AZO film can be attributed to the increase in both the electron concentration and the mobility. This result is intriguingly different from other degenerated semiconductors (highly doped semiconductors). In general, an increase in the doping concentration produces not only charge carriers but also ionized impurities. These ionized impurities work as scattering centers that reduce the carrier mobility significantly. On the aspect of the optical transmittance of pure AZO and Ag NP added AZO films (Figure 5), an increase in the content of Ag NPs up to 0.7 vol % does not change the transmittance of the

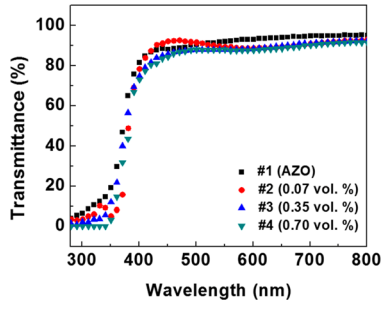

Figure 5. Optical transmittance of AZO and Ag NP added AZO films.

DOI: 10.1021/acsami.7b03871
ACS Appl. Mater. Interfaces 2017, 9, 19973−19979

mixture films noticeably. The transmittance of Ag NP added AZO film maintains over 85% in the visible wavelengths. This suggests that the small amount of Ag NPs does not cause significant scattering of incident light by the mixture films due to the small volume % of Ag NPs.

To understand the physical mechanism underlying the enhanced conductivity of Ag NP added AZO films, the concentration and mobility of electrons were characterized as a function of temperature. In addition to Ag NP added AZO films, pure AZO film and Ag film were included as control samples (Figure 6a). Moreover, the electric properties of Au

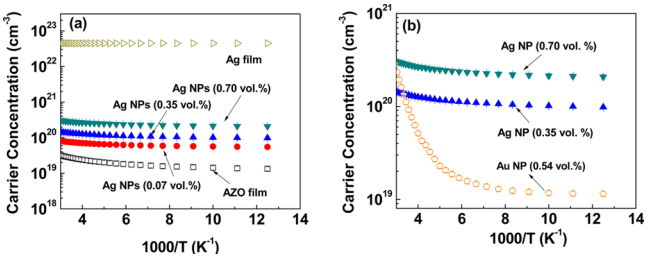

Figure 6. (a) Carrier concentrations of AZO:Ag NP mixture films as a function of temperature via the Hall effect measurements and (b) comparison in Arrhenius activation energies of Ag and Au NPs embedded AZO films with similar metal NP contents.

NP added AZO film (Au NP content: 0.54 vol %) were also measured to compare the effect of the metal work function on the electric properties of metal NP embedded AZO (Figure 6b). The electron concentration of Ag NP added AZO increases to 3×10^{20} cm^{-3} with increasing the content of Ag NPs. In addition, the temperature dependence of electron concentration is different between pure AZO film and Ag NP added AZO film. The Arrhenius plot shows that the activation energy of n vs $1/T$ of Ag NP added AZO films is ~11 meV, irrespective of Ag content. As for the electron concentration of pure AZO film, the activation energy of Al impurities is 20 meV, which corresponds to the energy required for the thermal excitation of electrons from Al impurity energy level to the conduction band edge.[23] Ag film in Figure 6a exhibits an activation energy close to 0 meV. This is consistent with electric properties of metals such as bulk Ag and Au. The electron concentration of metals is mainly determined by the valence states and their unit cell volume and is almost constant below room temperature. A difference in the temperature dependence of the electron concentration between Ag NP added AZO film, pure AZO film, and pure Ag film indicates that they have different free electron generation mechanisms. Because Ag NPs are isolated in the AZO matrix, the increase in the electron concentration by Ag NPs cannot be explained by the formation of a metallic Ag NP network. Furthermore, the trace amount of Ag NPs (0.07–0.7 vol %) in AZO is not sufficient to make a percolation path. Thus, this excludes the possibility that those electrons are conducting through the metallic network of adjacent Ag NPs.

Recently, we reported that the electron could be transferred from the embedded metal nanoparticles to the matrix through the thermionic emission.[22] The activation energy of the carrier concentration is attributed to the Schottky barrier at the metal–oxide interface. A barrier height is an offset of metal's work function and semiconductor's electron affinity. To examine the work function of AZO and Ag NPs of this study, ultraviolet photon emission (UPS) measurements were performed for pure AZO and Ag NP arrays in AZO. UPS results in Figure 7 shows that AZO film and Ag NP arrays have

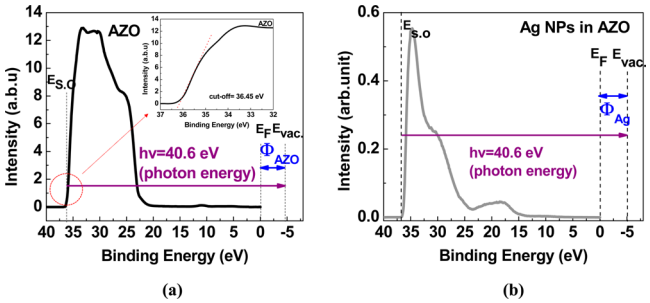

Figure 7. UPS results of (a) Ag NP array and (b) AZO film showing their Fermi energy (E_F) and their work functions.

the work functions of 4.15 and 4.24 eV, respectively. This is comparable with previous studies reporting the work function of AZO to be in the range of 3.7–4.7 eV[24] and that of Ag to be 4.2–4.6 eV.[25] Larger work functions of Ag NPs results in a Schottky barrier which prevents electron flow from Ag NPs to AZO, and the work function difference between Ag NPs and AZO explains the activation energy (11 meV) of n vs $1/T$ curve. In addition, larger Ag–AZO interfacial area in the mixture film of higher Ag NP content accelerates donation of more electrons to AZO matrix, leading to higher electron concentration. To study the role of Schottky junction at metal nanoparticle–AZO matrix, we also added Au NPs into AZO film and examined its electron concentration. Because the work function of Au (4.8–5.4 eV) is larger than that of Ag (4.3–4.7 eV), a higher Schottky junction barrier is expected at the Au–AZO interface.[25] In Figure 6b, n vs $1/T$ curve of Au NP (0.54 vol %) added AZO is compared with that of Ag NP (0.35 and 0.7 vol %) added AZO film. The activation energy for Au NP added AZO film is 54 meV above 180 K, which is 4.2 times larger than that of Ag NP added AZO film. It is noted that the thermal activation of electron donation is valid above 180 K. The activation energy decreases below 180 K in both Ag and Au NP added AZO. A change in the activation energy is attributed to a transition of the electron donation mechanism from a thermionic emission to a tunneling, which was reported in our previous study.[22] Consequently, the electron concentration of Au NP added AZO film increases 20 times as the temperature increases from 200 to 333 K, while Ag NP added AZO film exhibits only 30% increase in the electron concentration for the same temperature change. Because the work function of Au is 50–60 meV larger than that of Ag, a difference in the activation energy of n vs $1/T$ curve between Ag NP added and Au NP added AZO films confirms that electrons can be donated into the semiconductor matrix through the thermionic emission at the metal–semiconductor interface. On the basis of experimental results above, the electron donation mechanism is schematically explained in Figure 8.

We also examined the electron mobility of AZO films as a function of temperature. The electron mobility in Figure 9 is in the range from 10 to 20 cm^2 V^{-1}·s^{-1}, which is comparable to or better than that of electron-rich AZO films synthesized by sol–gel method.[1,26] Arrhenius plots (electron mobility vs $1/T$) of pure AZO and 0.07 vol % Ag NP added AZO film exhibit similar slopes in the temperature range from 200 to 340 K. This suggests that the electron scattering mechanism is the same for

DOI: 10.1021/acsami.7b03871
ACS Appl. Mater. Interfaces 2017, 9, 19973–19979

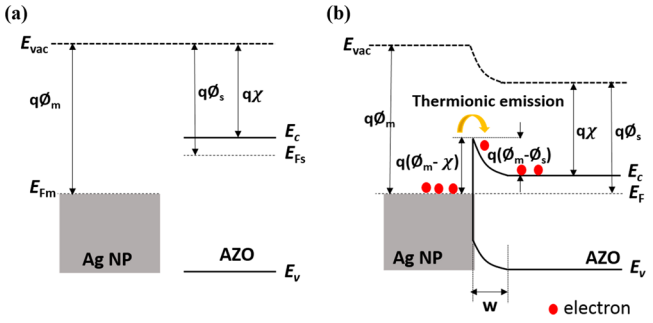

Figure 8. (a) Ag NP and AZO band diagrams before contact and (b) the equilibrium band diagram and the Schottky barrier formed at the Ag–AZO interface.

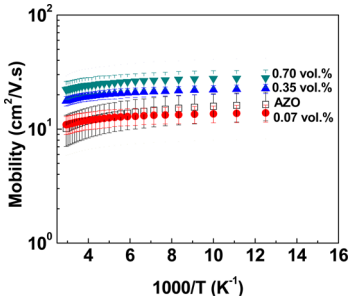

Figure 9. Hall mobility of mixture films as a function of temperature.

these two samples. Once electrons are donated to the AZO matrix, electrons travel through only AZO matrix and impurities. This transport behavior is very different from metal NW/TCO films and other TCO/metal/TCO sandwiched films where the metal component is a major electron transport path.[20,21] It is noted that an increase in Ag NPs content increases the electron mobility as well as the electron concentration. Results in Figure 9 are not consistent with previous studies, which show that donor impurities in degenerate TCO semiconductors add free electrons but decrease the electron mobility due to electron-impurity scatterings.[27] We explain the increase in the mobility of 0.7 and 1.4 vol % added AZO film from the standpoint of the ionized impurity deactivation. As Ag NPs increase the electron concentration, the Fermi level of the Ag NP added films gradually rises toward the conduction band edge. Figure 10 schematically shows that a change in the Fermi level from E_{F1} toward E_{F2} leaves the donor energy level (D°) below the Fermi

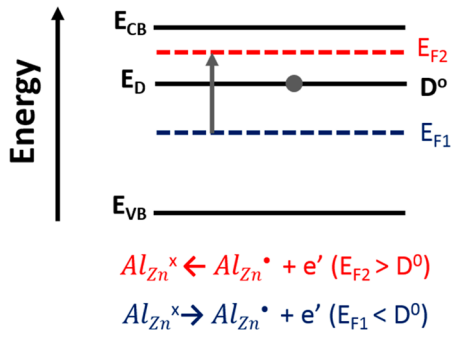

Figure 10. Band diagram of AZO showing that defect formation is governed by the relative position of Fermi level and the donor impurity level.

energy level of the mixture film. Then, the Fermi energy level becomes higher than D°, and the probability for the activation of donor impurities decreases. This suggests that donor impurities which would have been activated in pure AZO film become deactivated and neutralized in Ag NP added AZO. In comparison to activated impurities, the neutral impurities have much smaller electron scattering cross section, and the effect of Al impurities on the mobility of AZO matrix is reduced.[28,29] The reduced scattering of Al impurities by the increase in the Fermi energy level results in the higher mobility of 0.7 and 1.4 vol % Ag NP added AZO films.

The increased mobility is partially attributed to a decrease in the grain boundary scattering effect. Because the energy barrier at the grain boundary also scatters charge carriers, excess electrons can passivate the grain boundary barrier and suppress the scattering. This also increases the electron mobility. Optical mobility measurement may clearly show a relative contribution of the defect neutralization and the grain boundary scattering.

CONCLUSION

The electric properties of AZO films containing well-dispersed Ag NPs with the size of 21 ± 8.0 nm were studied. All films were synthesized via simple wet chemistry techniques. Ag NPs in the mixture films remain metallic without being oxidized and increase the electron concentration of the mixture film to 4×10^{20} cm^{-3}. In addition, the electron mobility of the mixture film is also doubled, although the electron concentration is increased by an order of magnitude. Temperature dependent electron concentration and the comparison of Ag NPs and Au NPs show the fact that the effect of Ag NP addition is due to the electron transfer from Ag NPs to the AZO matrix through the Schottky barrier (~11 meV) at the Ag–AZO interface. This electron doping by Ag NPs increases the Fermi energy level of the AZO film without changing the impurity concentration. Then, Al impurities are neutralized and their scattering power is reduced. Consequently, Ag NP added AZO film exhibits the electron mobility of 20 cm^2 $V^{-1}\cdot s^{-1}$ at the electron concentration of 3×10^{20} cm^{-3}, which is higher than the mobility of pure AZO film. Our study shows a new carrier donation mechanism for the design of highly electrically conductive degenerated semiconductors, which are useful for TCO applications.

EXPERIMENTAL SECTION

Preparation of AZO Sol. The starting precursor for AZO film was a mixture of zinc acetate dehydrate ($Zn(O_2CCH_3)_2\cdot 2H_2O$, 99.99%) and aluminum(III) nitrate nonahydrate ($Al(NO_3)_3\cdot 9H_2O$, ≥98%) that was dissolved in 2-methoxyethanol ($CH_3O(CH_2)_2OH$, 99.8%). Monoethanolamine (MEA, $NH_2(CH_2)_2OH$, 98%) was also added as a sol stabilizer, and the ratio of [MEA]/[Zn] was fixed at 1. The starting precursor was stirred at 80 °C until a clear solution was obtained. Then, the precursor was cooled to room temperature and set aside for 1 day for aging before further mixing with Ag colloidal solutions.

Synthesis of Ag Nanoparticles. Undesired agglomeration of Ag NPs was frequently observed during the synthesis process.[30−32] Instead of adding common surfactants such as polyvinylpyrrolidone (PVP), we used cellulose fibers as a solid template to mediate the chemical reduction of metal salt. The surface of the cellulose fibers contains many hydroxide groups that anchor metal species and prevent abrupt release of the metal species.[33−36] Thus, the Ag NPs and their agglomeration by the surfactants are significantly inhibited, which results in uniform Ag NPs well dispersed in liquid medium. The silver nitrate ($AgNO_3$, 99.9999%) was dissolved in the deionized water with the resistance of 18.3 MΩ. A piece of cellulose fiber paper was soaked

DOI: 10.1021/acsami.7b03871
ACS Appl. Mater. Interfaces 2017, 9, 19973−19979

in $AgNO_3$ aqueous solution for 10 min to adsorb Ag ions. This fabric piece was later gently dipped in the dilute sodium borohydride aqueous solution ($NaBH_4$, 98%). Released Ag ions were reduced to Ag NPs, and the color of the solution immediately turned into citrus orange. By repeating the soaking and dipping process several times, the initial Ag NP contents in colloidal solutions were varied from 0.01 to 0.05 M estimated by the Beer–Lambert's law without changing the size of Ag NPs. Then, Ag NPs were collected via centrifuging and were redispersed in 2-methoxyethanol. This chemical reduction method with assistance of cellulose fibers is illustrated in Figure 1.

AZO Films Containing Ag Nanoparticles. Ag NP alcoholic solution was mixed with AZO sol and aged for 1 day. Ag NP-AZO mixture solutions with different Ag content were spin-coated at a rate of 3000 rpm on soda-lime glass substrates repeatedly until the thickness of 200 nm was achieved (Figure S1). Glass substrates were sonicated in acetone and ethanol for 10 min in sequence and dried in the fume hood. Ag NP-AZO films were dried on a hot plate and annealed in nitrogen at 500 °C followed by the second treatment in N_2/H_2 mixture gas at 400 °C. The ramping rate of this thermal annealing was 2 °C min^{-1}.

Characterization. The Ag NP size and size distribution were measured using TEM (2000-CX, JEOL) and DLS LB550, Horiba) techniques. The TEM specimen was prepared by dropping 10 μL of Ag NP colloid solution onto a TEM copper grid. The crystal structures of the pure and Ag NP added AZO films were examined by GAXRD (X'Pert, PaNalytical) with Co Kα radiation of λ = 0.179 nm. The surface morphology of the films was characterized using AFM (Dimension 3100, Vecco). In addition, the chemical compositions of Ag NP added AZO films and the oxidation state of Ag NPs were investigated by the EPMA (JXA-8530F, JEOL) and XPS (ESCALAB 250Xi, Thermo Scientific). Ag contents of mixture films were also estimated by XPS and EPMA measurements. Ag contents in the film are summarized in Table 1. EPMA analysis shows that Ag content is 0.07, 0.35, and 0.7 vol %, which is close to the results of XPS analysis. Furthermore, the band structures at the Ag–AZO interfaces were studied by UPS (ESCALAB 250Xi, Thermo Scientific) equipped with a UV source of He II ($h\nu$ = 40.6 eV). Sheet resistance of the mixture films was characterized by the four-point probe method. Electron concentration and mobility in the mixture films were characterized using Hall effect measurements (HMS-5000, Ecopia) as a function of temperature. Measurements were performed in a dark condition to exclude the possibility of electron emission from surface plasmonic resonance. The temperature was elevated from 200 to 340 K (−73 to 68 °C) with an interval of 10 K. Magnetic field of 0.5 T was applied to the films during Hall effect measurements. The optical transmittance of the mixture films was also measured by UV–vis spectrometer (Lambda35, PerkinElmer) equipped with an integrating sphere.

■ ASSOCIATED CONTENT

Supporting Information

The Supporting Information is available free of charge on the ACS Publications website at DOI: 10.1021/acsami.7b03871.

SEM image, GAXRD pattern, and optical transmittance of both pure AZO and Ag NPs added AZO film (PDF)

■ AUTHOR INFORMATION

Corresponding Author

*E-mail: jul37@pitt.edu.

ORCID

Jung-Kun Lee: 0000-0002-7778-7679

Notes

The authors declare no competing financial interest.

■ ACKNOWLEDGMENTS

The authors appreciate Dr. Yong-Seop Park at Kyunghee University for his useful discussion on UPS measurement and data analysis. This work was supported by National Science Foundation (Grants CMMI-1333182 and EPMD-1408025) and the Global Frontier R&D Program on Center for Multiscale Energy System, Korea (Grant 2012M3A6A7054855).

■ REFERENCES

(1) Lin, J.-P.; Wu, J.-M. The Effect of Annealing Processes on Electronic Properties of Sol-Gel Derived Al-Doped ZnO Films. *Appl. Phys. Lett.* **2008**, *92*, 134103.

(2) Tsang, W. M.; Wong, F. L.; Fung, M. K.; Chang, J. C.; Lee, C. S.; Lee, S. T. Transparent Conducting Aluminum-Doped Zinc Oxide Thin Film Prepared by Sol-Gel Process Followed by Laser Irradiation Treatment. *Thin Solid Films* **2008**, *517*, 891–895.

(3) Shirakata, S.; Sakemi, T.; Awai, K.; Yamamoto, T. Electrical and Optical Properties of Large Area Ga-Doped ZnO Thin Films Prepared by Reactive Plasma Deposition. *Superlattices Microstruct.* **2006**, *39*, 218–228.

(4) Chen, K. J.; Hung, F. Y.; Chang, S. J.; Hu, Z. S. Microstructures, Optical and Electrical Properties of In-Doped ZnO Thin Films Prepared by Sol-Gel Method. *Appl. Surf. Sci.* **2009**, *255*, 6308–6312.

(5) Yu, Q.; Fu, W.; Yu, C.; Yang, H.; Wei, R.; Sui, Y.; Liu, S.; Liu, Z.; Li, M.; Wang, G.; Shao, C.; Liu, Y.; Zou, G. Structural, Electrical and Optical Properties of Yttrium-Doped ZnO Thin Films Prepared by Sol-Gel Method. *J. Phys. D: Appl. Phys.* **2007**, *40*, 5592.

(6) Liu, H.; Avrutin, V.; Izyumskaya, N.; Özgür, Ü.; Morkoç, H. Transparent Conducting Oxides for Electrode Applications in Light Emitting and Absorbing Devices. *Superlattices Microstruct.* **2010**, *48*, 458–484.

(7) Nguyen, N. G.; Ho, V. T. T.; Hong, L.-S. Low-Resistivity, High-Transmittance Ga:ZnO Films Prepared Through Metalorganic Chemical Vapor Deposition Using an Inexpensive Solution of Diethylzinc in *N*-Hexane as the Zn Precursor. *Appl. Phys. Lett.* **2013**, *102*, 181912.

(8) Gonçalves, G.; Elangovan, E.; Barquinha, P.; Pereira, L.; Martins, R.; Fortunato, E. Influence of Post-Annealing Temperature on the Properties Exhibited by ITO, IZO and GZO Thin Films. *Thin Solid Films* **2007**, *515*, 8562–8566.

(9) Janotti, A.; Van de Walle, C. G. Fundamentals of Zinc Oxide as a Semiconductor. *Rep. Prog. Phys.* **2009**, *72*, 126501.

(10) Ellmer, K. Resistivity of Polycrystalline Zinc Oxide Films: Current Status and Physical Limit. *J. Phys. D: Appl. Phys.* **2001**, *34*, 3097.

(11) Cohen, D. J.; Barnett, S. A. Predicted Electrical Properties of Modulation-Doped ZnO-Based Transparent Conducting Oxides. *J. Appl. Phys.* **2005**, *98*, 053705.

(12) Ellmer, K.; Vollweiler, G. Electrical Transport Parameters of Heavily-Doped Zinc Oxide and Zinc Magnesium Oxide Single and Multilayer Films Heteroepitaxially Grown on Oxide Single Crystals. *Thin Solid Films* **2006**, *496*, 104–111.

(13) Lee, S.; Bang, S.; Park, J.; Park, S.; Ko, Y.; Jeon, H. AZO/Au/AZO Multilayer as a Transparent Conductive Electrode. *Phys. Status Solidi A* **2012**, *209*, 698–701.

(14) Sivaramakrishnan, K.; Alford, T. L. Conduction and Transmission Analysis in Gold Nanolayers Embedded in Zinc Oxide for Flexible Electronics. *Appl. Phys. Lett.* **2010**, *96*, 201109.

(15) Indluru, A.; Alford, T. L. Effect of Ag Thickness on Electrical Transport and Optical Properties of Indium Tin Oxide-Ag-Indium Tin Oxide Multilayers. *J. Appl. Phys.* **2009**, *105*, 123528.

(16) Han, H.; Theodore, N. D.; Alford, T. L. Improved Conductivity and Mechanism of Carrier Transport in Zinc Oxide with Embedded Silver Layer. *J. Appl. Phys.* **2008**, *103*, 013708.

(17) Houng, B. Tin Doped Indium Oxide Transparent Conducting Thin Films Containing Silver Nanoparticles by Sol-Gel Technique. *Appl. Phys. Lett.* **2005**, *87*, 251922.

(18) Gao, T.; Li, Z.; Huang, P.-S.; Shenoy, G. J.; Parobek, D.; Tan, S.; Lee, J.-K.; Liu, H.; Leu, P. W. Hierarchical Graphene/Metal Grid

Structures for Stable, Flexible Transparent Conductors. *ACS Nano* **2015**, *9*, 5440−5446.
(19) Gao, T.; Huang, P.-S.; Lee, J.-K.; Leu, P. W. Hierarchical Metal Nanomesh/Microgrid Structures for High Performance Transparent Electrodes. *RSC Adv.* **2015**, *5*, 70713−70717.
(20) Kim, A.; Won, Y.; Woo, K.; Jeong, S.; Moon, J. All-Solution-Processed Indium-Free Transparent Composite Electrodes Based on Ag Nanowire and Metal Oxide for Thin-Film Solar Cells. *Adv. Funct. Mater.* **2014**, *24*, 2462−2471.
(21) Kim, A.; Won, Y.; Woo, K.; Kim, C.-H.; Moon, J. Highly Transparent Low Resistance ZnO/Ag Nanowire/ZnO Composite Electrode for Thin Film Solar Cells. *ACS Nano* **2013**, *7*, 1081−1091.
(22) Huang, P.-H.; Kim, D. H.; Lee, J.-K. Electron Emission of Au Nanoparticles Embedded in ZnO for Highly Conductive Oxide. *Appl. Phys. Lett.* **2014**, *104*, 142102.
(23) Hur, T. B.; Hwang, Y. H.; Kim, H. K.; Park, H. L. Study of the Structural Evolution in ZnO Thin Film by *In Situ* Synchrotron X-Ray Scattering. *J. Appl. Phys.* **2004**, *96*, 1740.
(24) Feng, Q.; Wang, W.; Jiang, K.; Huang, J.; Zhang, Y.; Song, W.; Tan, R. Effect of Deposition Condition and UV-Ozone Post-Treatment on Work Function of DC Magnetron Sputtered AZO Thin Films. *J. Mater. Sci.: Mater. Electron.* **2012**, *23*, 267−272.
(25) Uda, M.; Nakamura, A.; Yamamoto, T.; Fujimoto, Y. Work Function of Polycrystalline Ag, Au and Al. *J. Electron Spectrosc. Relat. Phenom.* **1998**, *88*−*91*, 643−648.
(26) Lin, K.-M.; Chen, H.-C.; Chen, Y.-Y.; Chou, K.-Y. Influences of Preferred Orientation Growth on Electrical Properties of ZnO:Al Films by Sol-Gel Method. *J. Sol-Gel Sci. Technol.* **2010**, *55*, 369−376.
(27) Lee, H.-C. Electron Scattering Mechanisms in Indium-Tin-Oxide Thin Films Prepared at the Various Process Conditions. *Appl. Surf. Sci.* **2006**, *252*, 3428−3435.
(28) Agashe, C.; Kluth, O.; Hupkes, J.; Zastrow, U.; Rech, B.; Wuttig, M. Efforts to Improve Carrier Mobility in Radio Frequency Sputtered Aluminum Doped Zinc Oxide Films. *J. Appl. Phys.* **2004**, *95*, 1911.
(29) Pei, Z. L.; Sun, C.; Tan, M. H.; Xiao, J. Q.; Guan, D. H.; Huang, R. F.; Wen, L. S. Optical and Electrical Properties of Direct-Current Magnetron Sputtered ZnO:Al Films. *J. Appl. Phys.* **2001**, *90*, 3432.
(30) Chou, K.-S.; Ren, C.-Y. Synthesis of Nanosized Silver Particles by Chemical Reduction Method. *Mater. Chem. Phys.* **2000**, *64*, 241−246.
(31) Chou, K.-S.; Huang, K.-C.; Lee, H.-H. Fabrication and Sintering Effect on the Morphologies and Conductivity of Nano-Ag Particle Films by the Spin Coating Method. *Nanotechnology* **2005**, *16*, 779.
(32) Qin, Y.; Ji, X.; Jing, J.; Liu, H.; Wu, H.; Yang, W. Size Control Over Spherical Silver Nanoparticles by Ascorbic Acid Reduction. *Colloids Surf., A* **2010**, *372*, 172−176.
(33) Barud, H. S.; Barrios, C.; Regiani, T.; Marques, R. F. C.; Verelst, M.; Dexpert-Ghys, J.; Messaddeq, Y.; Ribeiro, S. J. L. Self-Supported Silver Nanoparticles Containing Bacterial Cellulose Membranes. *Mater. Sci. Eng., C* **2008**, *28*, 515−518.
(34) Son, W. K.; Youk, J. H.; Park, W. H. Antimicrobial Cellulose Acetate Nanofibers Containing Silver Nanoparticles. *Carbohydr. Polym.* **2006**, *65*, 430−434.
(35) He, J.; Kunitake, T.; Nakao, A. Facile *In Situ* Synthesis of Noble Metal Nanoparticles in Porous Cellulose Fibers. *Chem. Mater.* **2003**, *15*, 4401−4406.
(36) Kotel'nikova, N. E.; Demidov, V. N.; Wegener, G.; Windeisen, E. Mechanisms of Diffusion-Reduction Interaction of Microcrystalline Cellulose and Silver Ions. *Russ. J. Gen. Chem.* **2003**, *73*, 427−433.

DOI: 10.1021/acsami.7b03871
ACS Appl. Mater. Interfaces 2017, 9, 19973−19979